Mitochondria Targeted and Intracellular Biothiol Triggered Hyperpolarized 129Xe Magnetofluorescent Biosensor

Qingbin Zeng,[†,‡,||] Qianni Guo,[†,‡,||] Yaping Yuan,[†,‡] Yuqi Yang,[†] Bin Zhang,[†] Lili Ren,[†] Xiaoxiao Zhang,[†] Qing Luo,[†,‡] Maili Liu,[†,‡] Louis-S. Bouchard,[§] and Xin Zhou*,[†,‡] [ID]

[†]Key Laboratory of Magnetic Resonance in Biological Systems, State Key Laboratory of Magnetic Resonance and Atomic and Molecular Physics, National Center for Magnetic Resonance in Wuhan, Collaborative Innovation Center of Chemistry for Life Sciences, Wuhan Institute of Physics and Mathematics, Chinese Academy of Sciences, Wuhan 430071, People's Republic of China

[‡]University of Chinese Academy of Sciences, Beijing 100049, People's Republic of China

[§]California Nano Systems Institute, Jonsson Comprehensive Cancer Center, The Molecular Biology Institute, Departments of Chemistry and Biochemistry and of Bioengineering, University of California, Los Angeles California 90095, United States

S *Supporting Information*

ABSTRACT: Biothiols such as gluthathione (GSH), cysteine (Cys), homocysteine (Hcy), and thioredoxin (Trx) play vital roles in cellular metabolism. Various diseases are associated with abnormal cellular biothiol levels. Thus, the intracellular detection of biothiol levels could be a useful diagnostic tool. A number of methods have been developed to detect intracellular thiols, but sensitivity and specificity problems have limited their applications. To address these limitations, we have designed a new biosensor based on hyperpolarized xenon magnetic resonance detection, which can be used to detect biothiol levels noninvasively. The biosensor is a multimodal probe that incorporates a cryptophane-A cage as 129Xe NMR reporter, a naphthalimide moiety as fluorescence reporter, a disulfide bond as thiol-specific cleavable group, and a triphenylphosphonium moiety as mitochondria targeting unit. When the biosensor

interacts with biothiols, disulfide bond cleavage leads to enhancements in the fluorescence intensity and changes in the 129Xe chemical shift. Using Hyper-CEST (chemical exchange saturation transfer) NMR, our biosensor shows a low detection limit at picomolar (10^{-10} M) concentration, which makes a promise to detect thiols in cells. The biosensor can detect biothiol effectively in live cells and shows good targeting ability to the mitochondria. This new approach not only offers a practical technique to detect thiols in live cells, but may also present an excellent in vivo test platform for xenon biosensors.
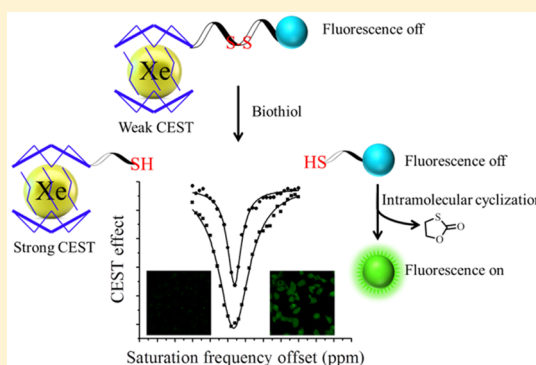
Biothiols play important roles in cell growth, apoptosis inhibition, DNA synthesis, and angiogenesis.[1,2] Some biothiols of interest include cysteine (Cys), homocysteine (Hcy), and thioredoxin (Trx). Another biothiol, gluthathione (GSH), is mainly found in the cytoplasm (1–10 mM) and is regarded as critically important to the operation of the mitochondria.[3–5] Mitochondria regulate cellular metabolism through the production of ATP. In mitochondria, GSH participates in the maintenance of the redox state of cells and circumvents oxidative damage, which can lead to cellular dysfunction and cell death.[6] Abnormal biothiol levels in mitochondria are directly correlated to the occurrence of cancer, Alzheimer's disease, Parkinson's disease, and cardiovascular disease.[7–9] Thus, it would be desirable and perhaps critically important to develop methods to detect mitochondrial thiols levels in living systems. A number of studies have reported detection of intracellular thiols.[10–13] However, the sensitivity and poor penetration depth have limited their applications. Magnetic resonance imaging (MRI), which is a powerful tool for the early detection of disease, features high spatial resolution and deep tissue penetration.[14] Recently, the

detection of GSH by ^{1}H MRI has been reported.[15,16] Unfortunately, ^{1}H MRI was found to lack the sensitivity required to detect physiologically relevant changes in GSH levels. One possible way to boost the sensitivity of MRI detection is to use hyperpolarization techniques. This usually involves the development of a suitable molecular probe that binds to a molecule of interest in order to report on it. And in terms of signal detection, NMR-sensitive nuclei such as [3]He, ^{13}C, [83]Kr, and [129]Xe are among those that have been used in hyperpolarization experiments.[17]

[129]Xe is a nontoxic inert gas whose nuclear spins possess a chemical shift that is sensitive to the local molecular environment in which it resides. It is particularly suited to biomedical applications because of the ability to dissolve xenon in the bloodstream.[18] The signal from hyperpolarized [129]Xe is 10 000-fold larger than that from thermal polarization,[19–21]

Scheme 1. Synthetic Route of Cryptophane Biosensor 7
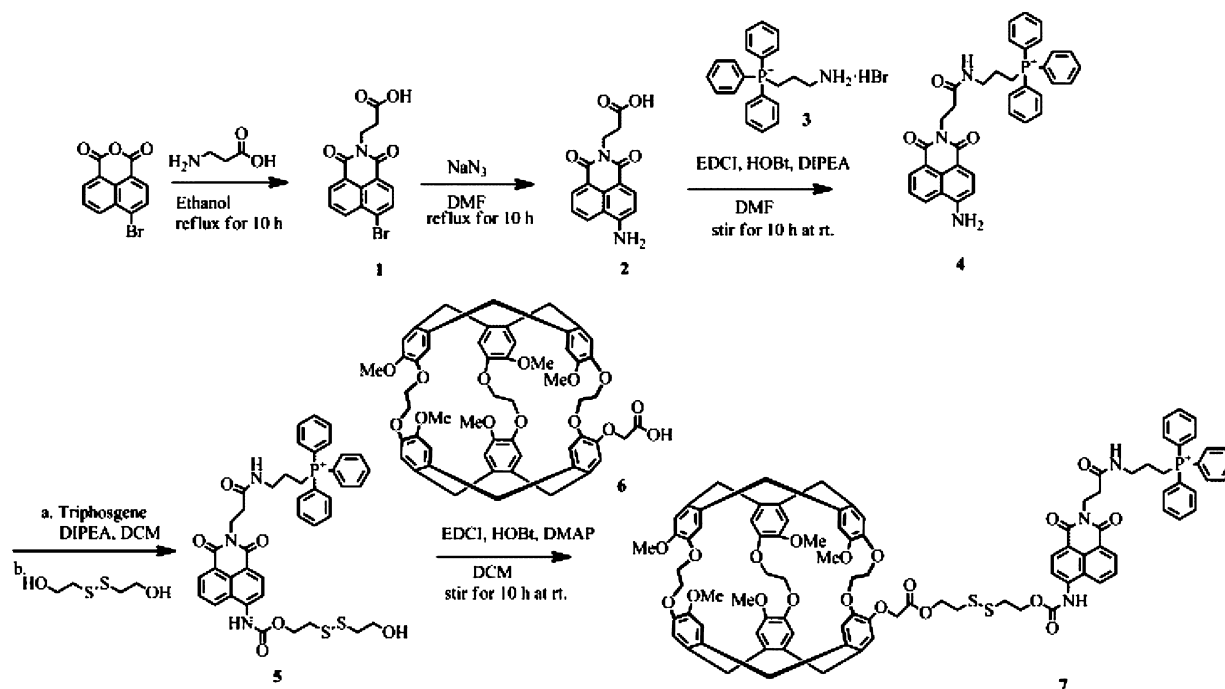
thereby enabling in vivo MRI of low-concentration tracer molecules, as demonstrated by many studies in rodents and humans.[22−25] Xenon can nonspecifically interact with proteins, lipids, spores, and shows high affinity for a family of host molecules called cryptophanes. Cryptophanes are very popular in host−guest chemistry.[26] The cryptophane-A cage provides the highest xenon affinity (4000 M^{-1}, in organic solvent) and exchange kinetics (the residence time range is 30−300 ms, in aqueous solution) so far among all the existing cryptophanes,[18] making it an excellent host for xenon atoms. In order to develop xenon MRI for detection of specific molecules, the cryptophane-A cage must be functionalized. Spence and co-workers first reported a functionalized xenon biosensor with high detection sensitivity exhibiting specific interactions with avidin.[27] However, the detection sensitivity of the xenon biosensor with hyperpolarization alone is insufficient to achieve molecular imaging of most biologically relevant molecules that are found in living systems. To overcome this sensitivity problem, a new method termed Hyper-CEST was developed.[28] The latter combines hyperpolarization together with the chemical exchange saturation transfer (CEST) method. This combination improves the sensitivity of the xenon biosensor by orders of magnitude, reaching sensitivity levels that now allow for molecular imaging.[29,30]

In recent years, a wide range of xenon biosensors based on cryptophane-A have been developed for the detection of pH,[31,32] proteins,[33−35] enzymes,[36,37] nucleic acids,[38] metal ions,[39−42] and transmembrane receptor targets.[17,30,43−45] Recently, additional host molecules have been developed, such as nanoemulsion,[46] perfluoroctyl bromide,[47] gas vesicles,[48] cucurbituril,[49−53] and protein.[54] However, there was only one report on the detection of biothiols in vitro based on a xenon biosensor.[55] Herein we report a mitochondria-targeting fluorescence/Xe-NMR multimodal cryptophane-A functionalized biosensor that allows for the detection of biothiols in live cells. As described below, this new biosensor composed of a host molecule (cryptophane-A), a disulfide-linker (linker), a

fluorescence moiety (naphthalimide), and a targeting group (triphenylphosphonium). The triphenylphosphonium is an effective mitochondrial-targeting site that can also increase the hydrophilic character of the sensor,[6] and whose disulfide bond is expected to be cleaved when the biosensor is exposed to biothiols. The 4-amino-1,8-naphthalimides have excellent spectroscopic characteristics, including large Stokes shift, high fluorescence quantum yield, and excellent internal charge transfer (ICT). These features led to its success as a fluorescent reporter. The cryptophane-A biosensor was synthesized following the synthetic route shown in Scheme 1.

EXPERIMENTAL SECTION

Synthesis. *Synthesis of Compound 1.* 4-Bromonaphthalic anhydride (3 g, 10 mmol) was dispersed in 20 mL of ethanol, and then 3-aminopropanoic acid (0.98 g, 11 mmol) was added to the mixture. After the mixture was refluxed for 10 h a precipitate was formed. The resulting mixture was cooled to room temperature, filtered, and the filter cake was washed by ethanol three times to give compound **1** as a gray solid (3.1 g, 89%). ^{1}H NMR (500 MHz, DMSO-d_6) δ: 8.55 (d, J = 7.3 Hz, 1H), 8.52 (dd, J = 8.4, 0.7 Hz, 1H), 8.31 (d, J = 7.8 Hz, 1H), 8.20 (d, J = 7.9 Hz, 1H), 7.98 (dd, J = 8.3, 7.5 Hz, 1H), 4.38−4.10 (m, 2H), 2.60 (m, 2H). ^{13}C NMR (125 MHz, DMSO-d_6) δ: 172.95, 163.10, 163.05, 1132.99, 131.92, 131.70, 131.28, 130.06, 129.59, 129.12, 128.52, 122.98, 122.20, 36.35, 32.61. HRMS (ESI): $[M + H]^+$ calcd for $C_{15}H_{11}BrNO_4$ m/z, 347.9871; found, 347.9868.

Synthesis of Compound 2. Compound **1** (1 g, 2.87 mmol) was dissolved in DMF (20 mL), and then NaN$_3$ (0.28 g, 4.31 mmol) was added. After refluxing for 10 h, the solvent was removed under vacuum. The residue was purified by silica gel column chromatography using DCM/MeOH (v/v 10/1) as eluent to give compound **2** as a brown solid (640 mg, 79%). ^{1}H NMR (500 MHz, DMSO-d_6) δ: 8.62 (d, J = 8.3 Hz, 1H), 8.42 (d, J = 7.0 Hz, 1H), 8.18 (d, J = 8.3 Hz, 1H), 7.68−7.60 (t, 1H), 7.46 (s, 2H), 6.84 (d, J = 8.4 Hz, 1H), 4.28−4.09 (t, 2H),

2.32−2.16 (t, 2H). ^{13}C NMR (125 MHz, DMSO-d_6) δ: 173.51, 164.16, 163.23, 153.31, 134.40, 131.49, 130.14, 129.97, 124.40, 122.06, 119.77, 108.62, 107.78, 35.98, 33.25. HRMS (ESI): [M + H]$^+$ calcd for $C_{15}H_{13}BrN_2O_4$ m/z, 285.0875; found, 285.0873.

Synthesis of Compound 3. 3-Bromopropylamine hydrobromide (0.77 g, 3.5 mmol) was dissolved in 1-butanol (10 mL), after the solution was degassed by bubbling N_2 for 10 min, triphenylphosphonium (1 g, 3.8 mmol) was added, the mixture was degassed for another 10 min and then heated at 120 °C under N_2 atmosphere for 12 h. After completion of the reaction, the solution was poured into methyl t-butyl ether (30 mL) and toluene (20 mL). After stirring at room temperature until a homogeneous slurry was obtained, the slurry was filtered and the filter cake was rinsed two times with methyl t-butyl ether (2 × 5 mL) to yield compound **3** as a white solid (1 g, 59.4%). ^{1}H NMR (500 MHz, DMSO-d_6) δ: 7.93 (m, 3H), 7.89−7.71 (m, 15H), 3.84−3.66 (m, 2H), 3.08−2.92 (m, 2H), 1.95−1.77 (m, 2H). ^{13}C NMR (125 MHz, DMSO-d_6) δ: 135.58, 134.14, 134.06, 130.91, 130.81, 118.86, 118.18, 20.55, 19.02, 18.60. HRMS (ESI): [M − HBr]$^+$ calcd for $C_{21}H_{23}NP^+$ m/z, 320.1568; found, 320.1582.

Synthesis of Compound 4. Compound **2** (100 mg, 0.35 mmol) was dissolved in DMF (5 mL), and then EDCI (222 mg, 1.16 mmol) and DMAP (141.5 mg, 1.16 mmol) were added. The mixture was stirred at room temperature for 30 min, and then compound **3** (168 mg, 0.35 mmol) was added. After stirring the solution at room temperature for another 10 h, the solvent was removed under vacuum. The residue was purified by silica gel column chromatography using DCM/MeOH (v/v 15/1) as eluent to give compound **4** as a yellow solid (140 mg, 60%). ^{1}H NMR (500 MHz, DMSO-d_6) δ: 8.61 (d, J = 8.4 Hz, 1H), 8.29 (d, J = 7.2 Hz, 1H), 8.05 (d, J = 8.2 Hz, 2H), 7.96−7.88 (m, 3H), 7.84−7.74 (m, 12H), 7.61 (t, J = 7.8 Hz, 1H), 7.46 (s, 2H), 6.79 (d, J = 8.4 Hz, 1H), 4.21 (t, J = 7.4 Hz, 2H), 3.56 (t, J = 14.2 Hz, 2H), 3.19 (dd, J = 13.3, 7.1 Hz, 2H), 2.41 (t, J = 7.4 Hz, 2H), 1.60−1.72 (m, 2H). ^{13}C NMR (125 MHz, DMSO-d_6) δ: 170.80, 164.19, 163.27, 153.23, 135.45, 134.30, 134.10, 134.02, 131.35, 130.81, 130.71, 130.17, 129.84, 124.40, 122.22, 119.81, 119.17, 118.49, 108.60, 107.92, 36.65, 34.57, 22.66, 19.02, 18.61. HRMS (ESI): [M]$^+$ calcd for $C_{36}H_{33}N_3O_3P^+$ m/z, 586.2260; found, 586.2288.

Synthesis of Compound 5. Compound **4** (100 mg, 0.15 mmol) and triphosgene (134 mg, 0.45 mmol) were dispersed in dry DCM (5 mL), and then DIPEA (136 mg, 1.05 mmol) was added dropwise in the solution under N_2 atmosphere. After the solution was stirred at room temperature for 3 h, the unreacted phosgene gas (Caution: toxic) was removed by bubbling N_2 in the solution and neutralization in a bath of NaOH. After that, a solution of 2,2′-dithiodiethanol (116 mg, 0.75 mmol) in DCM/THF (v/v 1/1) was added to the mixture. After the solution was stirred at room temperature for another 10 h, the solvent was evaporated under vacuum. The crude product was purified by silica gel column chromatography using DCM/MeOH (v/v 20/1) as eluent to give compound **5** as a yellow solid (60 mg, 48%). ^{1}H NMR (500 MHz, DMSO-d_6) δ: 8.56 (d, J = 8.4 Hz, 1H), 8.31 (d, J = 7.1 Hz, 1H), 8.17 (d, J = 8.2 Hz, 1H), 7.98 (d, J = 8.2 Hz, 1H), 7.90 (m, 3H), 7.81−7.68 (m, 13H), 4.49 (t, J = 5.8 Hz, 2H), 4.27 (t, J = 6.3 Hz, 2H), 3.70 (t, J = 6.2 Hz, 2H), 3.39 (d, J = 14.8 Hz, 2H), 3.20 (t, J = 6.3 Hz, 2H), 3.10 (t, J = 5.9 Hz, 2H), 2.87 (t, J = 6.2 Hz, 2H), 2.49 (t, J = 6.2 Hz, 2H), 1.64 (m, 2H). ^{13}C NMR(125 MHz, DMSO-d_6) δ: 170.67, 163.90, 163.35, 154.39, 141.12, 135.46, 134.10, 134.03, 131.94,

131.27, 130.81, 130.73, 129.90, 128.82, 126.89, 124.51, 122.74, 119.11, 118.54, 117.71, 65.41, 63.47, 59.89, 41.53, 37.04, 34.35, 22.62, 18.94, 18.60. HRMS (ESI): [M]$^+$ calcd for $C_{41}H_{41}N_3O_3PS_2^+$ m/z, 766.2174, found 766.2185.

Synthesis of Compound 6. Compound **6** was prepared as described in refs 27 and 38. Cryptophanol-A (100 mg, 0.113 mmol) and ethyl 2-bromoacetate (38.4 mg, 0.23 mmol) were dissolved in 15 mL of acetone, and then K_2CO_3 (77.4 mg, 0.56 mmol) was added. After the mixture was refluxed for 6 h, the mixture was cooled to room temperature, and 20 mL of ethyl acetate was added. The organic phase was washed with water (30 mL × 3) and dried with anhydrous Na_2SO_4, and the solvent was evaporated under vacuum to yield a white solid. The solid was dispersed in 20 mL of 3 M NaOH aqueous THF (1/1), and then the solution was cooled to room temperature after refluxing for 10 h. Subsequently, HCl (0.1 M) was added dropwise until the solution became neutral, DCM (30 mL) was then added, and the organic layer was washed with water and dried with anhydrous Na_2SO_4, and the solvent was evaporated under vacuum to yield the white solid as cryptophane **6** (83 mg, 78.3%). The product was taken to the next step without further purification. ^{1}H NMR (500 MHz, CDCl$_3$) δ: 6.87−6.62 (m, 12H), 4.65−4.53 (m, 6H), 4.38−4.12 (m, 11H), 4.08−3.96 (m, 3H), 3.91 (s, 3H), 3.85−3.73 (m, 12H), 3.48−3.37 (m, 6H). ^{13}C NMR (125 MHz, CDCl$_3$) δ: 170.92, 149.76, 149.67, 149.57, 149.47, 148.51, 147.92, 147.81, 146.95, 146.77, 146.73, 146.69, 146.10, 135.69, 134.79, 134.60, 134.05, 133.98, 133.70, 133.53, 133.02, 131.93, 131.68, 131.16, 131.05, 122.75, 122.32, 121.42, 120.87, 120.78, 120.57, 120.01, 114.46, 113.81, 113.66, 113.41, 69.98, 69.69, 69.27, 69.10, 69.03, 68.93, 67.98, 55.80, 55.76, 55.67, 55.56, 53.44, 36.29, 36.20. HRMS (ESI): [M − H]$^-$ calcd for $C_{55}H_{53}O_{14}$ m/z, 937.3435; found, 937.3449.

Synthesis of Compound 7. Compound **6** (25 mg, 0.027 mmol) was dissolved in dry DCM (5 mL), and then EDCI (15.5 mg, 0.081 mmol) was added to the solution. This was followed by stirring of the mixture at 0 °C for 30 min and addition of HOBt (10.9 mg, 0.081 mmol) to the mixture. We then stirred for another 1 h. After that, compound **5** (22.9 mg, 0.027 mmol) and DMAP (9.9 mg, 0.081 mmol) were added to the solution. After the solution was stirred at room temperature for another 10 h, the solvent was evaporated under vacuum. The crude product was purified by silica gel column chromatography using DCM/MeOH (v/v 20/1) as eluent to give compound **7** as a yellowish solid (8 mg, 16.8%). ^{1}H NMR (500 MHz, CDCl$_3$) δ: 8.85 (br, 1H), 8.37 (d, J = 10 Hz, 1H), 8.29−8.20 (m, 2H), 8.16 (d, J = 10 Hz, 1H), 8.12 (s, 1H), 7.86−7.66 (m, 15H), 7.52 (t, J = 8 Hz, 1H), 6.80−6.60 (m, 12H), 4.68−4.42 (m, 14H), 4.26−4.06 (m, 12H), 3.83−3.69 (m, 17H), 3.51−3.27 (m, 9H), 3.10 (m, 3H), 2.83 (m, 2H), 1.90 (m, 2H). ^{13}C NMR (125 MHz, CDCl$_3$) δ: 170.67, 168.74, 163.92, 163.42, 154.40, 149.88, 149.74, 149.70, 149.64, 149.45, 147.89, 147.61, 146.80, 146.77, 146.65, 146.61, 141.23, 135.47, 134.26, 134.19, 134.16, 134.14, 134.07, 133.99, 133.96, 133.94, 133.84, 131.97, 131.81, 131.68, 131.58, 131.53, 131.31, 131.19, 130.76, 130.68, 129.88, 128.80, 126.93, 123.49, 122.69, 121.61, 121.27, 121.24, 120.79, 120.05, 119.06, 118.51, 118.28, 117.69, 114.62, 113.74, 113.69, 113.64, 69.55, 69.47, 69.42, 69.38, 69.33, 69.04, 67.23, 65.48, 63.49, 61.22, 59.84, 56.14, 55.80, 55.76, 55.67, 55.56, 53.44, 41.53, 37.11, 36.23, 36.08, 34.35, 22.55, 18.94, 18.54. HRMS (ESI): [M]$^+$ calcd for $C_{96}H_{93}N_3O_{19}PS_2^+$ m/z, 1687.5616; found, 1687.5630.

Spectra Studies. For all biologically relevant analytes [Val, Leu, Ile, Phe, Trp, Met, Pro, Gly, Ser, Thr, Tyr, Asn, Gln, His,

Lys, Arg, Asp, Glu, Ala, Cys, Hcy, GSH, K^+, Mg^{2+}, Fe^{2+}, Ca^{2+}, Cu^{2+}, Mn^{2+}, Zn^{2+}], stock solutions were prepared in ultrapure water. The stock solution for biosensor **7** was prepared in spectral grade DMSO. Absorption spectra were obtained on a Thermo Scientific evolution 220 UV−vis spectrometer, and fluorescence spectra were recorded on an Edinburgh FS5 fluorescence spectrophotometer. The samples for absorption and fluorescence experiments were stored in quartz cuvettes (3 mL volume). The excitation wavelength was 440 nm, and the excitation and emission slit widths were kept at 4 nm. All spectra were acquired in PBS buffer (pH = 7.4, 20 mM) and 20% DMSO (v/v).

^{129}Xe NMR Studies. Hyperpolarized ^{129}Xe gas was generated by a home-built ^{129}Xe hyperpolarizer. All ^{129}Xe NMR experiments were obtained using a 400 MHz Bruker AV400 wide-bore spectrometer (Bruker Biospin, Ettlingen, Germany). A gas mixture of 10% N_2, 88% He, and 2% Xe (86% enriched ^{129}Xe or natural abundance ^{129}Xe) was flowed through the hyperpolarizer. The gas was directly bubbled into a 10 mm NMR tube for 20 s, and then the spectrum was obtained. Sample temperature was controlled by VT unit on NMR spectrometer to 298 K. Spectra were acquired in PBS buffer (pH = 7.4, containing 50% DMSO) using 16 scans. NMR spectra for direct detected were processed using a 10 Hz line broadening filter. For the Hyper-CEST NMR experiment, after the gas mixture flowed through the hyperpolarizer, the gas was directly bubbled into a 10 mm NMR tube for 20 s, followed by a 3 s delay to allow the bubbles to collapse. Afterward, continuous wave (CW) pulses were used to selectively saturate the Xe@cryptophane cage peak. This was followed by the acquisition of a spectrum. Each spectrum was acquired in a single scan. NMR spectra for CEST were processed using 6 Hz line broadening filter.

Cellular Fluorescence Imaging Studies. Human lung cancer cells H1299 were incubated in RPMI-1640 supplemented with 10% fetal bovine serum and 1% penicillin−streptomycin at 37 °C in 5% CO_2 and 95% ir environment. The cells were seeded on 6-well plates and stabilized overnight. Biosensor **7** was applied to the cells to monitor its uptake, as discussed in the main text above. In some experiments, the cells were incubated with media containing Mito-Tracker red (Lyso-Tracker red or ER-Tracker red or NEM) prior to treatment with biosensor **7**. The cells were then briefly washed with 1 mL of PBS and treated with biosensor **7** in PBS. After incubation, residual quantities of biosensor **7** not taken up by the cells were removed by washing the cells three times with PBS before the cells were placed in 1 mL of a PBS solution. Fluorescence images were taken on a Nikon confocal laser scanning microscope.

Cellular Hyper-CEST Spectra Studies. Human lung cancer cells H1299 were incubated in RPMI-1640 supplemented with 10% fetal bovine serum and 1% penicillin−streptomycin at 37 °C in 5% CO_2 and 95% ir environment. The cells were incubated with biosensor **7** [biosensor **7** (30 μM) and dissolved in culture medium (including 1% DMSO, 1% Cremophor EL)] for 2 h. The cells were washed three times with PBS at room temperature, followed by trypsinization and resuspension in culture medium. The cell concentration was kept at 1.29×10^7 cells/mL. Finally, the cells were transferred to an NMR tube, and the ^{129}Xe NMR spectra were acquired by CEST. The cells of the control group were incubated with N-ethylmaleimide (NEM) for 2 h. Residual quantities of NEM not taken up by the cells were removed by washing the cells

three times with PBS. The cells were then incubated with biosensor **7** for another 2 h. Other procedures were carried out similarly to the case of the experimental group. For CEST experiment, a selective saturation pulse was swept across the chemical shift range of 55−85 ppm in 1 ppm steps (CW saturation for 10 s with a 6.0 μT field). The temperature was set to 298 K.

RESULTS AND DISCUSSION

Spectroscopy Studies. We first tested the spectroscopic properties of biosensor **7**. As shown in Figure 1, after addition
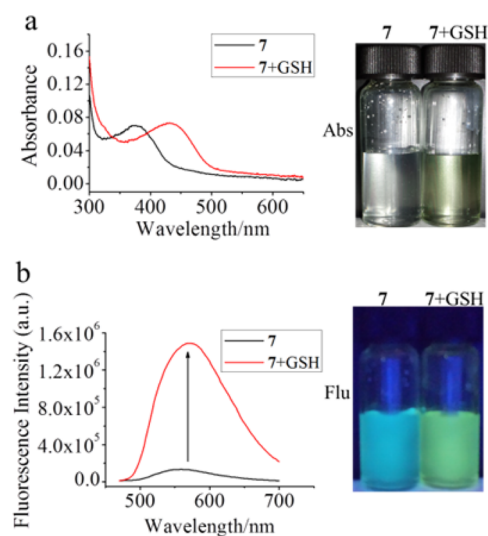
Figure 1. Optical spectra and photos of biosensor **7** (5 μM) recorded in the presence and absence of GSH (2.5 mM). (a) Absorption spectra (black line, in the absence of GSH; red line, in the presence of GSH). (b) Fluorescence spectra (black line, in the absence of GSH; red line, in the presence of GSH). All spectra and photographs were acquired at room temperature after incubation at 37 °C for 2 h in PBS buffer (pH = 7.4, 20 mM), containing 20% DMSO (v/v).

of 500 equiv GSH to the solution and heating for 2 h at 37 °C, the absorption spectra appeared red-shifted by 70 nm, going from 375 to 445 nm (Figure 1a), whereas the color of the solution changed from colorless to yellow. Meanwhile, the fluorescence intensity at 560 nm was enhanced 11-fold (Figure 1b) while the fluorescence changed from blue to green-yellow. The products of biosensor **7** reacted with GSH were analyzed by liquid chromatography−mass spectrometry (LC−MS) (Figure S1). We found that, after reacting biosensor **7** with GSH, a peak appeared at m/z 613.1597 (Figure S1b), which corresponds to GSSG. We also found an m/z value of 586.2267 (Figure S1c) for the peak of compound **4**. These results demonstrate that biosensor **7** can be reduced by GSH, releasing compound **4**, while the GSH is oxidized to yield GSSG. The proposed reaction mechanism for the biosensor reacting with biothiols is shown in Scheme S1. A disulfide bond is cleaved followed by intramolecular rearrangement, which leads to the activation of the fluorescent moiety. These results demonstrate that the signal from the cryptophane-A biosensor is modulated by GSH.

The selectivity and stability of biosensor **7** were tested in solution. We found the fluorescence intensity at 560 nm to be enhanced severalfold upon the addition of biothiols (Figure 2a) such as GSH, Cys, and Hcy. On the other hand, there were no
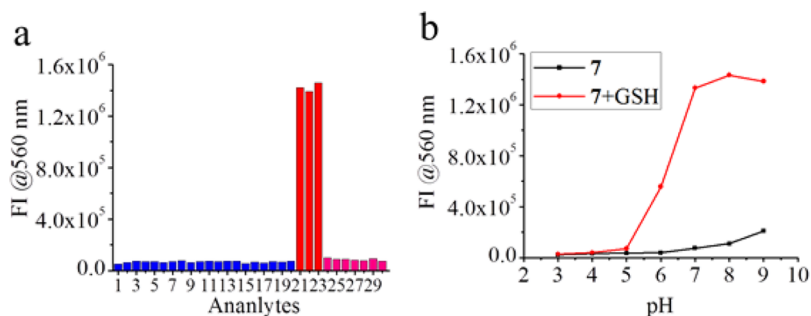
Figure 2. Fluorescence response of biosensor **7** (5 μM) to different analytes and pH. (a) Fluorescence intensity at 560 nm response of biosensor **7** (5 μM) for non-thiol amino acids (1, only biosensor; 2, Val; 3, Leu; 4, Ile; 5, Phe; 6, Trp; 7, Met; 8, Pro; 9, Gly; 10, Ser; 11, Thr; 12, Tyr; 13, Asn; 14, Gln; 15, His; 16, Lys; 17, Arg; 18, Asp; 19, Glu; 20, Ala), biothiols (21, Cys; 22, Hcy; 23, GSH), and biologically essential metal ions (24, K^+; 25, Mg^{2+}; 26, Fe^{2+}; 27, Ca^{2+}; 28, Cu^{2+}; 29, Mn^{2+}; 30, Zn^{2+}). The concentration of non-thiol amino acids, biothiols, and essential metal ions were kept at 500 μM. (b) Fluorescence response of biosensor **7** (5 μM) with and without GSH as a function of pH. All spectra were acquired at room temperature after heating to 37 °C for 2 h in PBS buffer (20 mM) with 20% DMSO (v/v).

significant changes observed with the addition of other non-thiol amino acids or biologically essential metal ions. The biosensor shows high stability across a broad range of pH values (Figure 2b). The response of biosensor **7** was stable across the pH range of 3−8; however, its fluorescence intensity at 560 nm is pH-dependent in the presence of GSH. When GSH is present, the fluorescence intensity at 560 nm is enhanced severalfold across the pH range of 6−9. These results lend support to the hypothesis that biosensor **7** can be used to detect intracellular thiols without obstruction from non-thiol amino acids, metal ions, and pH effects. We also tested the stability of biosensor **7** in serum solution. As shown in Figure S2, the biosensor appears to undergo slight changes after 3 h in serum. But this effect is negligible compared to the response of the biosensor reacting to biothiols.

Fluorescence spectra of biosensor **7** treated by different equivalents of GSH were acquired. As shown in Figure S3a, the fluorescence intensity is enhanced when the concentration of GSH is increased. When the concentration of GSH reached 200 μM (40 equiv), the fluorescence intensity showed no obvious further changes (Figure S3a, inset). This demonstrates that the reaction has reached completion at this concentration. Time-dependent fluorescence spectra were also acquired (Figure S3b). The latter show that the fluorescence intensity increases rapidly over the interval (0−10 min), whereas the fluorescence intensity at 560 nm almost linearly increased during the 0−5 min interval (Figure S3b, inset). Twenty minutes later, the fluorescence intensity attains a plateau, where the reaction reached completion. The kinetics of biosensor **7** treated by different equivalents of GSH are analyzed in Figure S4a. The reaction rate was found to correlate with GSH concentration. Similar results were observed upon the addition of Cys and Hcy to solution of biosensor **7** (Figure S4b). This biosensor shows fast response toward thiols; all the reactions completed after the thiols were added to the solution for 20 min.

^{129}Xe NMR Spectra Studies. To investigate how GSH can be monitored by ^{129}Xe NMR, ^{129}Xe NMR spectra of biosensor **7** were acquired. In Figure S5, biosensor **7** was dissolved in solution without heating and the xenon spectrum was acquired at room temperature. We find two different resonances: xenon in solution (234.3 ppm) and xenon in the cryptophane cage (71.5 ppm). After heating for 2 h at 37 °C, a new small signal appeared at 70.1 ppm, which may be indicative of sensor decomposition (Figure 3a). Signs of decomposition may also be observed in the fluorescence spectra. The GSH concen-
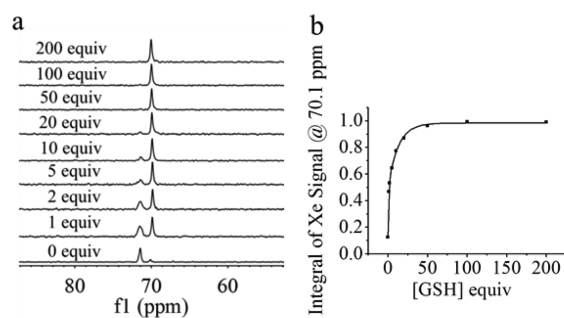
Figure 3. (a) ^{129}Xe NMR spectra (average of 16 scans, line broadening = 10 Hz) of biosensor **7** (25 μM) response to different equivalents of GSH. (b) Integral of ^{129}Xe NMR signal at 70.1 ppm. All spectra were acquired at room temperature after incubation at 37 °C for 2 h in PBS buffer (pH = 7.4, 20 mM), containing 50% DMSO (v/v).

tration dependence ^{129}Xe NMR spectra are shown in Figure 3. When the concentration of GSH is increased, the xenon signal intensity at 70.1 ppm increases, whereas that at 71.5 ppm decreases (see Figure 3a). This demonstrates that biosensor **7** reacts with GSH. The addition of GSH resulted in the chemical shift of caged Xe (Xe@ cryptophane-A) to shift by 1.4 ppm in the upfield direction. The upfield change of the chemical shift may be caused by a weak electron-withdrawal effect. Triphenylphosphonium is a positively charged moiety that can attract the electrons of xenon in the cage. While the disulfide bond of biosensor **7** is cleaved, the triphenylphosphonium functionalized aminonaphthalimide moiety is released from the biosensor, and the distance from the cage to the triphenylphosphonium moiety is increased. The electron-withdrawing effect of triphenylphosphonium is not effectively transferred to the encapsulated xenon. As a result, the electron cloud density of the encapsulated xenon is increased, leading to a shielding effect toward Xe@cryptophane-A. This leads to the observed upfield change in chemical shift of Xe@cryptophane-A following the reaction of the biosensor with GSH. ^{129}Xe NMR spectra of biosensor **7** collected as a function of GSH concentration are shown in Figure 3b. The Xe@cryptophane-A signal did not show further changes when the concentration of GSH reached 1.25 mM (50 equiv). This trend was consistent with the fluorescence spectra. This shows that the reaction reached completion.

We also investigated the ^{129}Xe NMR spectra of biosensor **7** treated by different analytes under the same conditions. We

found that in the presence of the Cys and Hcy, the Xe@ cryptophane-A signal intensity at 70.1 ppm is enhanced severalfold (Figure S6a), whereas [129]Xe NMR spectra were similar to the spectra of biosensor **7** treated with GSH. For biosensor **7** treated by other non-thiol amino acids, no new signal enhancements are observed at 70.1 ppm (Figure S6b). These results demonstrate that biosensor **7** exhibits good selectivity for thiols.

Hyper-CEST [129]Xe NMR. We also investigated the sensitivity of biosensor **7**. As shown in Figure S7, 1 μM biosensor **7** can produce 20% CEST signal, which is still at least 3−4 orders of magnitude more sensitive than ^{1}H CEST contrast agents.[56] To determine the detection threshold for biosensor **7**, we investigated dilutions of biosensor **7** to 50 nM, 500 pM, 200 pM, as well as a control solution containing 20 mM phosphate buffer. For each sample, we collected saturation profiles by employing saturation pulses at the Xe@cage frequency for incremental saturation times. As shown in Figure S8, the detection threshold of biosensor **7** is 200 pM. This low detection threshold implies that biosensor **7** and [129]Xe NMR have the potential for detecting thiols in cells at low concentration.

Cellular Fluorescence Imaging. To confirm whether biosensor **7** can selectively stain mitochondria, fluorescence imaging of cells was performed. Biosensor **7** and Mito-Tracker red (ER-Tracker red, Lyso-Tracker red) were incubated with human lung cancer cells (H1299). Mito-Tracker red is a fluorescent sensor for mitochondria. As seen in Figure 4 and
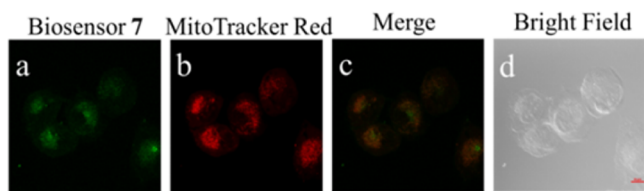
Figure 4. Fluorescence images of H1299 cells treated with biosensor **7** and Mito-Tracker red. After the cells were incubated with biosensor **7** (5.0 μM) at 37 °C for 20 min, the medium was replaced by fresh medium containing Mito-Tracker red (0.05 μM) and the cells were incubated for another 10 min. Images for biosensor **7** and Mito-Tracker red were obtained after excitation at 488 and 561 nm. (a) Biosensor **7**. (b) Mito-Tracker red. (c) Colocalization image. (d) Bright-field image. Scale bar, 10 μm.

Figure S9 (Supporting Information), the fluorescence emission of biosensor **7** overlaps well with that of the Mito-Tracker red compared to ER-Tracker red or Lyso-Tracker red. The colocalization coefficient (calculated use MATLAB 2011, data is shown in Table S1) of biosensor **7** with Mito-Tracker red was 0.72, which indicated that biosensor **7** is mainly found in mitochondria.

To investigate whether biosensor **7** can be used to detect biothiols in live cells, the cells were treated with NEM followed by biosensor **7**. NEM is a well-known agent which can block the thiol. As shown in Figure 5, in the presence of the agent the fluorescence intensity of cells treated with biosensor **7** decreased significantly. With the concentration of NEM increasing, the fluorescence intensity of the cells treated with biosensor **7** decreased gradually (Figure S10). These results prove that biosensor **7** can be used for biothiols detection in cells and has the potential for monitoring biothiols levels in live cells.
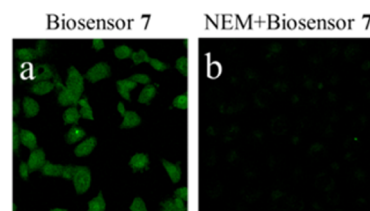
Figure 5. Fluorescence images of H1299 cells treated by NEM and biosensor **7**. (a) Cells incubated with biosensor **7**. (b) After the cells were incubated with NEM at 37 °C for 30 min, the medium was replaced by fresh medium containing biosensor **7** (5 μM) and the cells were incubated for another 30 min at 37 °C. Images for biosensor **7** were obtained after excitation at 488 nm.

Cellular Hyper-CEST [129]Xe NMR. Finally, to confirm whether cellular thiols can be monitored by [129]Xe NMR, the Hyper-CEST method was investigated in cell studies. Biosensor **7** (30 μM) was dissolved in culture medium (including 1% DMSO, 1% Cremophor EL), and then incubated with human lung cancer cells (H1299) in a culture flask at 37 °C. After 2 h of incubation the cells were washed and resuspended in culture medium, with the cell concentration held at 1.29×10^7 cells/ mL. In order to detect the signal of [129]Xe@cryptophane-A in cells, a selective saturation pulse was swept across the chemical shift range of 55−85 ppm in 1 ppm steps (CW saturation for 10 s with a 6.0 μT field). As shown in Figure 6, only one signal
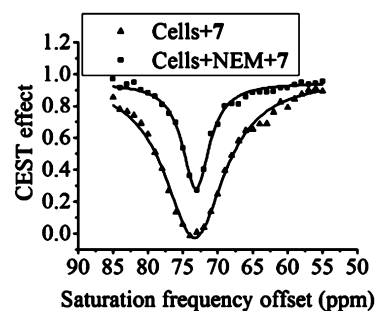
Figure 6. Hyper-CEST spectra for biosensor **7** in lung cancer cells (H1299). (▲) After the biosensor **7** was incubated with H1299 at 37 °C for 2 h, the Hyper-CEST spectrum was acquired. (■) After the H1299 cells were incubated with NEM at 37 °C for 2 h, the culture medium was replaced by fresh medium containing biosensor **7** (30 μM) and the cells were incubated for another 2 h, followed by the acquisition of a Hyper-CEST spectrum. All spectra were acquired at room temperature. Data were fitted with Lorentzian lines.

appeared around 73 ppm corresponding to [129]Xe@ crypto-phane-A in cells. In order to confirm whether biosensor **7** can be used to monitor biothiols levels in cells, NEM (3 mM) was used to block the cellular biothiols, followed by incubation of biosensor **7** with H1299 for 2 h. The remaining procedures were identical to the experimental group (i.e., cell concentration held at 1.29×10^7 cells/mL). We found that the signal of [129]Xe@ cryptophane-A was much smaller than for the experimental group, but the chemical shift exhibited almost no differences. Interestingly, at lower cell concentration (6.8×10^6 cells/mL) and lower NEM concentration (1 mM), we obtained the same results (Figure S11). At the same time, the Hyper-CEST spectra of biosensor **7** (5 μM) in PBS buffer including 50% DMSO (Figure S12) show that the CEST effect is increased upon interaction of biosensor **7** with GSH. After the biosensor is reacted with biothiols, the biosensor produced a

more water-soluble compound. So the CEST signal increased after the biosensor was reacted with biothiols (Table S2). These results demonstrate that biosensor **7** can be used to detect biothiols in cells by Hyper-CEST spectra.

CONCLUSIONS

In summary, we have developed a new biosensor to detect biothiols, which consists of a cryptophane-A cage, a disulfide-linker, and a triphenylphosphonium-functionalized naphthalimide group. This biosensor shows good stability across a broad range of pH values and can be used for the detection of biothiols. The triphenylphosphonium moiety endows the biosensor with the ability to selectively target mitochondria. While the biosensor reacts with free biothiols, the disulfide bond is cleaved, followed by intramolecular cyclization and a loss of the naphthalimide group. The loss of the naphthalimide group leads to an 11-fold enhancement of the fluorescence intensity of the biosensor. At the same time, the disulfide bond cleavage leads the chemical shift of the xenon atoms encapsulated in cryptophane-A cages to change by 1.4 ppm upfield. The detection threshold of biosensor **7** was found to be 200 pM, which makes its use to detect biothiols in cells at low concentration promising. The colocalization experiment demonstrated that the biosensor is localized to the mitochondria. More importantly, the cellular fluorescence images and Hyper-CEST spectra both demonstrate that the new biosensor can respond to biothiols in cells. This provides a new strategy for monitoring biothiols levels in cells. The development of xenon biosensors to enable the detection thiols in cells is a key step toward future in vivo applications. We envisage that this method could potentially be used for the detection biothiols levels in vivo. We are currently developing biosensors functionalized with peptides or polymers to improve the water solubility and bioavailability.

ASSOCIATED CONTENT

Ⓢ Supporting Information

The Supporting Information is available free of charge on the ACS Publications website at DOI: 10.1021/acs.anal-chem.6b03742.

Materials and instruments, LC−MS analysis, proposed mechanism of biosensor **7** reaction with biothiols, detection limit of biosensor **7**, cellular fluorescence imaging, and fluorescence, ^{129}Xe NMR, Hyper-CEST NMR, ^{1}H NMR, ^{13}C NMR, and ESI-HRMS spectra (PDF)

AUTHOR INFORMATION

Corresponding Author

*E-mail: xinzhou@wipm.ac.cn.

ORCID Ⓞ

Xin Zhou: 0000-0002-5580-7907

Author Contributions

‖Q.Z. and Q.G. contributed equally to this work.

Notes

The authors declare no competing financial interest.

ACKNOWLEDGMENTS

REFERENCES

(1) Zhang, S.; Ong, C. N.; Shen, H. M. *Cancer Lett.* **2004**, *208*, 143−153.
(2) Herzenberg, L. A.; DeRosa, S. C.; Dubs, J. G.; Roederer, M.; Anderson, M. T.; Ela, S. W.; Deresinski, S. C.; Herzenberg, L. A. *Proc. Natl. Acad. Sci. U. S. A.* **1997**, *94*, 1967−1972.
(3) Hong, R.; Han, G.; Fernandez, J. M.; Kim, B. J.; Forbes, N. S.; Rotello, V. M. *J. Am. Chem. Soc.* **2006**, *128*, 1078−1079.
(4) Hwang, C.; Sinskey, A. J.; Lodish, H. F. *Science* **1992**, *257*, 1496−1502.
(5) Wu, X.; Sun, X.; Guo, Z.; Tang, J.; Shen, Y.; James, T. D.; Tian, H.; Zhu, W. *J. Am. Chem. Soc.* **2014**, *136*, 3579−3588.
(6) Lim, C. S.; Masanta, G.; Kim, H. J.; Han, J. H.; Kim, H. M.; Cho, B. R. *J. Am. Chem. Soc.* **2011**, *133*, 11132−11135.
(7) Lee, M. H.; Han, J. H.; Kwon, P. S.; Bhuniya, S.; Kim, J. Y.; Sessler, J. L.; Kang, C.; Kim, J. S. *J. Am. Chem. Soc.* **2012**, *134*, 1316−1322.
(8) Shahrokhian, S. *Anal. Chem.* **2001**, *73*, 5972−5978.
(9) Seshadri, S.; Beiser, A.; Selhub, J.; Jacques, P. F.; Rosenberg, I. H.; D'Agostino, R. B.; Wilson, P. W. F.; Wolf, P. A. *N. Engl. J. Med.* **2002**, *346*, 476−483.
(10) Safavi, A.; Maleki, N.; Farjami, E.; Mahyari, F. A. *Anal. Chem.* **2009**, *81*, 7538−7543.
(11) Wang, Y.; Lu, J.; Tang, L.; Chang, H. X.; Li, J. *Anal. Chem.* **2009**, *81*, 9710−9715.
(12) Chen, X.; Zhou, Y.; Peng, X.; Yoon, J. Y. *Chem. Soc. Rev.* **2010**, *39*, 2120−2135.
(13) Niu, W.; Guo, L.; Li, Y.; Shuang, S.; Dong, C.; Wong, M. *Anal. Chem.* **2016**, *88*, 1908−1914.
(14) Terreno, E.; Delli Castelli, D.; Viale, A.; Aime, S. *Chem. Rev.* **2010**, *110*, 3019−3042.
(15) Zhao, Z.; Fan, H.; Zhou, G.; Bai, H.; Liang, H.; Wang, R.; Zhang, X.; Tan, W. *J. Am. Chem. Soc.* **2014**, *136*, 11220−11223.
(16) Chen, Y.; Xu, P.; Shu, Z.; Wu, M.; Wang, L.; Zhang, S.; Zheng, Y.; Chen, H.; Wang, J.; Li, Y.; Shi, J. *Adv. Funct. Mater.* **2014**, *24*, 4386−4396.
(17) Khan, N. S.; Riggle, B. A.; Seward, G. K.; Bai, Y. B.; Dmochowski, I. J. *Bioconjugate Chem.* **2015**, *26*, 101−109.
(18) Palaniappan, K. K.; Francis, M. B.; Pines, A.; Wemmer, D. E. *Isr. J. Chem.* **2014**, *54*, 104−112.
(19) Walker, T. G.; Happer, W. *Rev. Mod. Phys.* **1997**, *69*, 629−642.
(20) Zhou, X.; Sun, X.; Luo, J.; Zeng, X.; Liu, M.; Zhan, M. *Chin. Phys. Lett.* **2004**, *21*, 1501−1503.
(21) Zhou, X.; Graziani, D.; Pines, A. *Proc. Natl. Acad. Sci. U. S. A.* **2009**, *106*, 16903−16906.
(22) Zhou, X.; Mazzanti, M. L.; Chen, J. J.; Tzeng, Y. S.; Mansour, J. K.; Gereige, J. D.; Venkatesh, A. K.; Sun, Y.; Mulkern, R. V.; Albert, M. S. *NMR Biomed.* **2008**, *21*, 217−225.
(23) Zhou, X.; Sun, Y.; Mazzanti, M.; Henninger, N.; Mansour, J.; Fisher, M.; Albert, M. *NMR Biomed.* **2011**, *24*, 170−175.
(24) Mugler, J. P.; Altes, T. A. *J. Magn. Reson. Imaging* **2013**, *37*, 313−331.
(25) Qing, K.; Ruppert, K.; Jiang, Y.; Mata, J. F.; Miller, W.; Shim, Y. M.; Wang, C.; Ruset, I. C.; Hersman, F. W.; Altes, T. A.; Mugler, J. P. *J. Magn. Reson. Imaging* **2014**, *39*, 346−359.
(26) Little, M. A.; Donkin, J.; Fisher, J.; Halcrow, M. A.; Loder, J.; Hardie, M. J. *Angew. Chem., Int. Ed.* **2012**, *51*, 764−766.
(27) Spence, M. M.; Rubin, S. M.; Dimitrov, I. E.; Ruiz, E. J.; Wemmer, D. E.; Pines, A.; Yao, S.; Tian, F.; Schultz, P. G. *Proc. Natl. Acad. Sci. U. S. A.* **2001**, *98*, 10654−10657.
(28) Schröder, L.; Lowery, T. J.; Hilty, C.; Wemmer, D. E.; Pines, A. *Science* **2006**, *314*, 446−449.

(29) Klippel, S.; Dopfert, J.; Jayapaul, J.; Kunth, M.; Rossella, F.; Schnurr, M.; Witte, C.; Freund, C.; Schröder, L. *Angew. Chem., Int. Ed.* **2014**, *53*, 493−496.

(30) Rose, H. M.; Witte, C.; Rossella, F.; Klippel, S.; Freund, C.; Schröder, L. *Proc. Natl. Acad. Sci. U. S. A.* **2014**, *111*, 11697−11702.

(31) Berthault, P.; Desvaux, H.; Wendlinger, T.; Gyejacquot, M.; Stopin, A.; Brotin, T.; Dutasta, J. P.; Boulard, Y. *Chem. - Eur. J.* **2010**, *16*, 12941−12946.

(32) Riggle, B. A.; Wang, Y.; Dmochowski, I. J. *J. Am. Chem. Soc.* **2015**, *137*, 5542−5548.

(33) Schlundt, A.; Kilian, W.; Beyermann, M.; Sticht, J.; Gunther, S.; Hopner, S.; Falk, K.; Roetzschke, O.; Mitschang, L.; Freund, C. *Angew. Chem., Int. Ed.* **2009**, *48*, 4142−4145.

(34) Boutin, C.; Stopin, A.; Lenda, F.; Brotin, T.; Dutasta, J. P.; Jamin, N.; Sanson, A.; Boulard, Y.; Leteurtre, F.; Huber, G.; Bogaert-Buchmann, A.; Tassali, N.; Desvaux, H.; Carriere, M.; Berthault, P. *Bioorg. Med. Chem.* **2011**, *19*, 4135−4143.

(35) Kotera, N.; Dubost, E.; Milanole, G.; Doris, E.; Gravel, E.; Arhel, N.; Brotin, T.; Dutasta, J. P.; Cochrane, J.; Mari, E.; Boutin, C.; Leonce, E.; Berthault, P.; Rousseau, B. *Chem. Commun.* **2015**, *51*, 11482−11484.

(36) Wei, Q.; Seward, G. K.; Hill, P. A.; Patton, B.; Dimitrov, I. E.; Kuzma, N. N.; Dmochowski, I. J. *J. Am. Chem. Soc.* **2006**, *128*, 13274−13283.

(37) Chambers, J. M.; Hill, P. A.; Aaron, J. A.; Han, Z.; Christianson, D. W.; Kuzma, N. N.; Dmochowski, I. J. *J. Am. Chem. Soc.* **2009**, *131*, 563−569.

(38) Roy, V.; Brotin, T.; Dutasta, J. P.; Charles, M. H.; Delair, T.; Mallet, F.; Huber, G.; Desvaux, H.; Boulard, Y.; Berthault, P. *ChemPhysChem* **2007**, *8*, 2082−2085.

(39) Kotera, N.; Tassali, N.; Leonce, E.; Boutin, C.; Berthault, P.; Brotin, T.; Dutasta, J. P.; Delacour, L.; Traore, T.; Buisson, D. A.; Taran, F.; Coudert, S.; Rousseau, B. *Angew. Chem., Int. Ed.* **2012**, *51*, 4100−4103.

(40) Tassali, N.; Kotera, N.; Boutin, C.; Leonce, E.; Boulard, Y.; Rousseau, B.; Dubost, E.; Taran, F.; Brotin, T.; Dutasta, J. P.; Berthault, P. *Anal. Chem.* **2014**, *86*, 1783−1788.

(41) Zhang, J.; Jiang, W.; Luo, Q.; Zhang, X.; Guo, Q.; Liu, M.; Zhou, X. *Talanta* **2014**, *122*, 101−105.

(42) Guo, Q.; Zeng, Q.; Jiang, W.; Zhang, X.; Luo, Q.; Zhang, X.; Bouchard, L. S.; Liu, M.; Zhou, X. *Chem. - Eur. J.* **2016**, *22*, 3967−3970.

(43) Palaniappan, K. K.; Ramirez, R. M.; Bajaj, V. S.; Wemmer, D. E.; Pines, A.; Francis, M. B. *Angew. Chem., Int. Ed.* **2013**, *52*, 4849−4853.

(44) Rossella, F.; Rose, H. M.; Witte, C.; Jayapaul, J.; Schröder, L. *ChemPlusChem* **2014**, *79*, 1463−1471.

(45) Witte, C.; Martos, V.; Rose, H. M.; Reinke, S.; Klippel, S.; Schröder, L.; Hackenberger, C. P. R. *Angew. Chem., Int. Ed.* **2015**, *54*, 2806−2810.

(46) Stevens, T. K.; Ramirez, R. M.; Pines, A. *J. Am. Chem. Soc.* **2013**, *135*, 9576−9579.

(47) Klippel, S.; Freund, C.; Schroder, L. *Nano Lett.* **2014**, *14*, 5721−5726.

(48) Shapiro, M. G.; Ramirez, R. M.; Sperling, L. J.; Sun, G.; Sun, J.; Pines, A.; Schaffer, D. V.; Bajaj, V. S. *Nat. Chem.* **2014**, *6*, 629−634.

(49) Wang, Y.; Dmochowski, I. J. *Chem. Commun.* **2015**, *51*, 8982−8985.

(50) Kunth, M.; Witte, C.; Hennig, A.; Schroder, L. *Chem. Sci.* **2015**, *6*, 6069−6075.

(51) Schnurr, M.; Sloniec-Myszk, J.; Dopfert, J.; Schroder, L.; Hennig, A. *Angew. Chem., Int. Ed.* **2015**, *54*, 13444−13447.

(52) Wang, Y.; Roose, B. W.; Philbin, J. P.; Doman, J. L.; Dmochowski, I. J. *Angew. Chem., Int. Ed.* **2016**, *55*, 1733−1736.

(53) Slack, C. C.; Finbloom, J. A.; Jeong, K.; Bruns, C. J.; Wemmer, D. E.; Pines, A.; Francis, M. B. *Chem. Commun.* **2017**, *53*, 1076−1079.

(54) Wang, Y.; Roose, B. W.; Palovcak, E. J.; Carnevale, V.; Dmochowski, I. J. *Angew. Chem., Int. Ed.* **2016**, *55*, 8984−8987.

(55) Yang, S.; Jiang, W.; Ren, L.; Yuan, Y.; Zhang, B.; Luo, Q.; Guo, Q.; Bouchard, L. S.; Liu, M.; Zhou, X. *Anal. Chem.* **2016**, *88*, 5835−5840.

(56) Zhang, S.; Zhou, K.; Huang, G.; Takahashi, M.; Sherry, A. D.; Gao, J. *Chem. Commun.* **2013**, *49*, 6418−6420.